DOI: 10.1111/mice.12422

ORIGINAL ARTICLE

WILEY COMPUTER-AIDED CIVIL AND INFRASTRUCTURE ENGINEERING

Deep neural network with high-order neuron for the prediction of foamed concrete strength

Tuan Nguyen[1] | Alireza Kashani[1] | Tuan Ngo[1] | Stéphane Bordas[2,3]

[1]Department of Infrastructure Engineering, University of Melbourne, Melbourne, Australia

[2]Institute of Computational Engineering, University of Luxembourg, Luxembourg

[3]Department of Medical Research, China Medical University, Taichung, Taiwan

Correspondence
Tuan Ngo, Department of Infrastructure Engineering, University of Melbourne, Melbourne, Australia.
Email: dtngo@unimelb.edu.au

Funding information
ARC, Grant/Award Number: IC150100023

Abstract

The article presents a deep neural network model for the prediction of the compressive strength of foamed concrete. A new, high-order neuron was developed for the deep neural network model to improve the performance of the model. Moreover, the cross-entropy cost function and rectified linear unit activation function were employed to enhance the performance of the model. The present model was then applied to predict the compressive strength of foamed concrete through a given data set, and the obtained results were compared with other machine learning methods including conventional artificial neural network (C-ANN) and second-order artificial neural network (SO-ANN). To further validate the proposed model, a new data set from the laboratory and a given data set of high-performance concrete were used to obtain a higher degree of confidence in the prediction. It is shown that the proposed model obtained a better prediction, compared to other methods. In contrast to C-ANN and SO-ANN, the proposed model can genuinely improve its performance when training a deep neural network model with multiple hidden layers. A sensitivity analysis was conducted to investigate the effects of the input variables on the compressive strength. The results indicated that the compressive strength of foamed concrete is greatly affected by density, followed by the water-to-cement and sand-to-cement ratios. By providing a reliable prediction tool, the proposed model can aid researchers and engineers in mixture design optimization of foamed concrete.

1 | INTRODUCTION

Foamed concrete is a type of lightweight concrete that offers many advantages such as reducing the dead load of structures, improving sound and thermal insulation properties, and reducing transportation and installation costs (Ngo, Hajimohammadi, Sanjayan, & Mendis, 2017; Hajimohammadi, Ngo, & Mendis, 2017a; Nguyen, Ghazlan, Kashani, Bordas, & Ngo, 2018). These advantages make foamed concrete suitable for a myriad of applications in infrastructure construction and the prefabricated industry such as prefabricated blocks or panels, insulated walls, aircraft runway arrestors, roof decks, and geotechnical backfills. The use of foamed concrete poses a new challenge to perform its mixture design optimization that requires an accurate and quick understanding of the relationship between its properties and mixture proportions. Among the properties of foamed concrete, compressive strength is the most important in terms of its mechanical performance. Numerous studies have revealed that the compressive strength of foamed concrete decreases when its density decreases (Hajimohammadi et al., 2017b; Hajimohammadi, Ngo, Mendis, & Sanjayan, 2017c). Several researches have conducted studies to predict the compressive strength of foamed concrete based on mixture proportions. Most studies

are empirical, in which empirical equations were developed by calibrating experimental data as discussed in the following section. Predicting the compressive strength of foamed concrete using empirical equations is usually limited by a range of input conditions. Therefore, these predictions are generally extrapolative in practice (Nehdi, Djebbar, & Khan, 2001). Moreover, such semi-analytical models require the determination of empirical constants that are not easy to obtain to describe such complex relationships between mixture proportions and the compressive strength (Chiew, Ng, Chai, & Tay, 2017). Therefore, there is a significant need for the development of an advanced prediction tool.

This article presents a deep neural network (DNN) model, which is a subset of machine learning (ML), for the prediction and understanding of foamed concrete strength. ML and data science has shown great potential for predicting, designing, and discovering materials (Ley & Bordas, 2018). In civil engineering and construction, ML has been extensively used in a variety of applications such as structural heal monitoring (Gao & Mosalam, 2018; Rafiei & Adeli, 2017, 2018; Xue & Li, 2018), reliability analysis (Dai & Cao, 2017; Grande, Castillo, Mora, & Lo, 2017; Nabian & Meidani, 2018), transportation (Dharia & Adeli, 2003; García-Ródenas, López-García, & Sánchez-Rico, 2017; Yu, Wang, Shan, & Yao, 2018; Zhang & Ge, 2013), and prediction and estimation (Adeli & Wu, 1998; Chou & Pham, 2013; Rafiei, Khushefati, Demirboga, & Adeli, 2017a; Zhao & Ren, 2002). In concrete-related studies, DeRousseau, Kasprzyk, and Srubar (2018) recently reviewed the application of ML to optimize mixture design of concrete. This study suggested that ML methods are powerful tools for mixture design optimization because they are able to account for the complexity of mixtures and objective functions. Rafiei, Khushefati, Demirboga, and Adeli (2016) comprehensively reviewed different ML approaches to estimate the properties of concrete. Using a deep restricted Boltzmann machine, Rafiei, Khushefati, Demirboga, and Adeli (2017b) presented a mode to predict the compressive strength of concrete from 103 concrete test data retrieved from the ML repository of the University of California, Irvine. The estimated results by the deep restricted Boltzmann machine were compared with ANN and support vector machine (SVM) models. Combining artificial firefly algorithm and SVM method, Chou and Pham (2015) proposed a framework for predicting the compressive strength of normal concrete and high-strength concrete. Abd and Abd (2017) predicted the compressive strength of foamed concrete using a traditional multivariable nonlinear regression and revolutionary SVM. The results showed a good correlation between the actual compressive strength and predicted compressive strength. A model to predict the compressive strength of foamed concrete based on extreme learning machine (ELM) was proposed in Yaseen et al. (2018). The ELM model was subsequently validated in comparison with M5 Tree and SVM methods.

Recently, among different ML techniques, artificial neural network (ANN) has widely been used in civil engineering (Adeli & Panakkat, 2009; Panakkat & Adeli, 2009; Wang & Adeli, 2015). ANN was originally inspired by human brains in which information is transmitted and processed by biological neurons to build complicated concepts and ideas (Adeli, 2001). The architecture of conventional ANN consists of a input layer, a hidden layer, and a output layer. The connection of neurons from one layer to others was modeled by weights and biases through the linear inner product and activation function (Bui, Nguyen, Chou, Nguyen-Xuan, & Ngo, 2018). Sigmoid function is the most prevalent activation function in the conventional ANN model (C-ANN). To quantify the performance of the C-ANN, quadratic cost function is commonly used. Many advantages of the C-ANN were demonstrated for the prediction of concrete strength in the literature. For example, Naderpour, Rafiean, and Fakharian (2018) employed C-ANN with the sigmoid activation function and quadratic cost function to predict the compressive strength of recycled aggregate concrete. To do so, 139 concrete test data were retrieved from the literature to train and test the C-ANN model. Based on C-ANN approach, Sarıdemir (2009) developed a prediction tool for the compressive strength of concrete containing metakaolin and silica fume. Thirty-three different mixtures with 195 specimens were collected from the literature to construct the model. The compressive strength of expanded polystyrene (EPS) lightweight concrete was predicted by ANN models in Sadrmomtazi, Sobhani, and Mirgozar (2013). For foamed concrete strength, Nehdi et al. (2001) used the C-ANN model with eight hidden neurons (due to computational limitation) to forecast the strength of foamed concrete.

Despite many advantages, the C-ANN model suffers from several drawbacks such as learning slowdown problem due to the quadratic cost function and vanishing gradient problem due to the sigmoid activation function (Goodfellow, Bengio, & Courville, 2016; Nielsen, 2015). Moreover, it is known that the C-ANN only performs linear calculation between neurons in a layer through the inner product (Fan, Cong, & Wang, 2018). This forms a hypothesis that the inner product (i.e., linear neuron) in the C-ANN can be replaced by a quadratic function (second-order neuron) as presented in Fan et al. (2018). It is shown by Fan et al. (2018) that the new second-order ANN (SO-ANN) can successfully work for nonlinear function such as XOR gate and concentric rings that are unable to capture by the C-ANN with the linear neuron. Fan et al. (2018) concluded that the performance of the second-order model would be better than the C-ANN with the linear neuron. In fact, Roberts and Attoh-Okine (1998) alternatively used a simple quadratic ANN model to predict the International Roughness Index (IRI) for pavement assessment. Even though the quadratic model in Roberts and Attoh-Okine (1998) is quite simple and different to the one in Fan et al. (2018),

the quadratic model can capture the nonlinearity of this problem very well. It showed that the quadratic ANN model outperformed the linear ANN model in predicting the IRI.

Motivated by the literature, this study presents the DNN with high-order neuron to predict the compressive strength of foamed concrete. Inspired by the second-order model presented in Fan et al. (2018), the article proposes a general, high-order neuron for the DNN model (HO-DNN). Moreover, the cross-entropy cost and rectified linear unit (ReLU) activation functions are utilized to address the learning slowdown and vanishing gradient problems. The article is the first attempt to investigate the performance of HO-DNN model for real engineering applications. It is noticeable that Fan et al. (2018) only validated their SO-ANN model with mathematical functions (e.g., XOR, NAND, and NOR gates) and a shallow neural network with one hidden layer. The developed model was validated by predicting foamed concrete strength through a given data set. The obtained results were compared with other methods including C-ANN and SO-ANN. The model was further validated by a completely new data set from the laboratory and another given data set of high-performance concrete to obtain a higher level of validation. Having a reliable model, a sensitivity analysis (SA) was then performed to determine the effects of the input variables on the compressive strength of foamed concrete.

2 | EMPIRICAL EQUATIONS

This section briefly describes some empirical models reported in the literature. Interested readers are encouraged to refer to original publications for the detailed derivation of these models. Most empirical equations for the prediction of the compressive strength of foamed concrete are commonly based on three fundamental models, namely, Balshin's, Feret's, and Power's models (Neville, 2012). Balshin's model, which is known as the strength-porosity model (Kiani, Gandomi, Sajedi, & Liang, 2016), assumes that the compressive strength of concrete is affected by the volume of air voids in concrete (interlayer pores/spaces, gel pores, capillary pores, and entrapped air voids). Based on the strength-porosity model, Hoff (1972) first proposed an empirical equation as follows:

$$\sigma_y = \sigma_0 \left[\frac{d_c \left(1 + 0.2\rho_c\right)}{(1+k)\,\rho_c \gamma_w} \right]^b \tag{1}$$

in which σ_y is the compressive strength of foamed concrete; σ_0 is the theoretical compressive strength of cement paste at absolute zero porosity; d_c is the density of foamed concrete; k is the water-to-cement ratio (by weight); ρ_c is the specific gravity of ordinary Portland cement that is 3.15 as given in Hoff (1972); and γ_w is the unit weight of water. It is noted that σ_0 is impossible to obtain in practice; therefore, σ_0 and b are empirical constants that are determined by calibrating the model with experimental data. Based on the same approach, Nambiar and Ramamurthy (2008) established an empirical equation that takes into account the presence of sand as follows:

$$\sigma_y = \sigma_0 \left[\frac{d_c \left(1 + 0.2\rho_c + s_c^v\right)}{(1+k)\left(1 + s_c^w\right)\rho_c \gamma_w} \right]^b \tag{2}$$

in which s_c^w is the sand-to-cement ratio by weight and s_c^v is the sand-to-cement ratio by volume, which is calculated by $s_c^v = s_c^w \frac{\rho_c}{\rho_s}$; $\rho_c = 3.13$ and $\rho_s = 2.52$ are the specific gravity of cement and sand as given in Nambiar and Ramamurthy (2008). Similar to Hoff's model, σ_0 and b are empirical constants that require calibration.

Whilst Balshin's model is based on the porosity and the weights of the constituents, in Feret's model, the compressive strength of foamed concrete is governed by the absolute volume of its constituents as follows:

$$\sigma_y = K\left(\frac{c}{c+w+a}\right)^n \tag{3}$$

in which c, w, and a are the absolute volumes of cement, water, and air in the mixtures; K and n are empirical constants. Following Feret's model, Tam, Lim, Sri Ravindrarajah, and Lee (1987) calibrated Equation (3) to predict the compressive strength of foamed concrete with $K = 5{,}350$ and $n = 3.96$.

Power's models link the compressive strength of foamed concrete to the gel–space ratio as follows:

$$\sigma_y = k(g)^n \tag{4}$$

in which k is the intrinsic strength of the gel, n is an empirical constant, and g is the gel–space ratio. In Nambiar and Ramamurthy (2008), the formulation of the gel–space ratio (g) was derived as follows:

$$g = \frac{2.06\alpha V_c}{1 - V_{fl} - V_c\,(1-\alpha)} \tag{5}$$

in which V_c is the volume of cement, V_{fl} is the volume of the fillers, and α is the hydration parameter, which was assumed to be 0.8 (Nambiar & Ramamurthy, 2008). As porosity (or density) is the most important factor in foamed concrete strength, the strength-porosity models are prevalent in empirical equations for foamed concrete strength (Nguyen, Bui, Ngo, & Nguyen, 2017). Therefore, two empirical equations based on this model (Hoff, 1972; Nambiar & Ramamurthy, 2008) are used in this article.

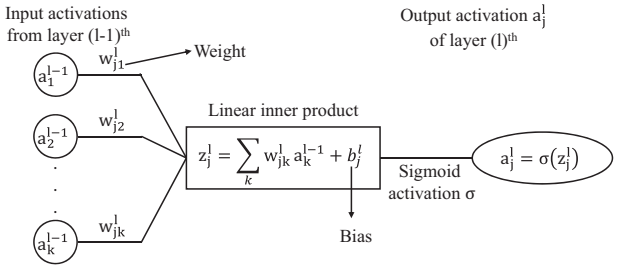

FIGURE 1 The structure of a linear neuron in C-ANN model

3 | DEEP NEURAL NETWORK WITH HIGH-ORDER NEURON

This section presents the development of the DNN for the prediction of foamed concrete strength with the high-order neuron, cross-entropy cost function, and ReLU activation function. In this article, the stochastic gradient decent-backpropagation (SGD-BP) algorithm is used to train the model because it is very effective for training neural network models. The SGD-BP algorithm only calculates and stores the gradient vector (first order) and does not require a Hessian matrix (second order). Therefore, the algorithm and its variants can deal with any general engineering problems, particularly DNNs. The detailed description of the SGD-BP algorithm can be found in the literature (Goodfellow et al., 2016; Nielsen, 2015).

3.1 | Conventional artificial neural network

Prior to the development of HO-DNN, the conventional ANN (C-ANN) is quickly reexamined in this section. The structure of a neuron in C-ANN is depicted in Figure 1. In C-ANN, input activations from the layer $(l-1)$th are transmitted to a neuron in the next layer by the linear inner product as depicted in Figure 1. The weighted input z_j^l (Figure 1) is then converted to the output activation a_j^l by the sigmoid activation function σ. To estimate the performance of C-ANN, the quadratic cost function $C_{\text{quadratic}}$ is commonly used in the literature as follows:

$$C_{\text{quadratic}} = \frac{1}{2}\left\|\boldsymbol{y} - \boldsymbol{a}^L\right\|^2 \tag{6}$$

where $\boldsymbol{y}$ is the vector of actual outputs corresponding to an input x and $\boldsymbol{a}^L$ is the vector of activations of the last (output) layer L when x is input. Using the SGD-BP algorithm and the chain rule, the C-ANN model can be trained by propagating backward errors at each layer, which are defined as follows (Nielsen, 2015):

$$\delta_j^L = \frac{\partial C_{\text{quadratic}}}{\partial z_j^L} = \frac{\partial C_{\text{quadratic}}}{\partial a_j^L}\sigma'\left(z_j^L\right) = \left(y_j - a_j^L\right)\sigma'\left(z_j^L\right) \tag{7}$$

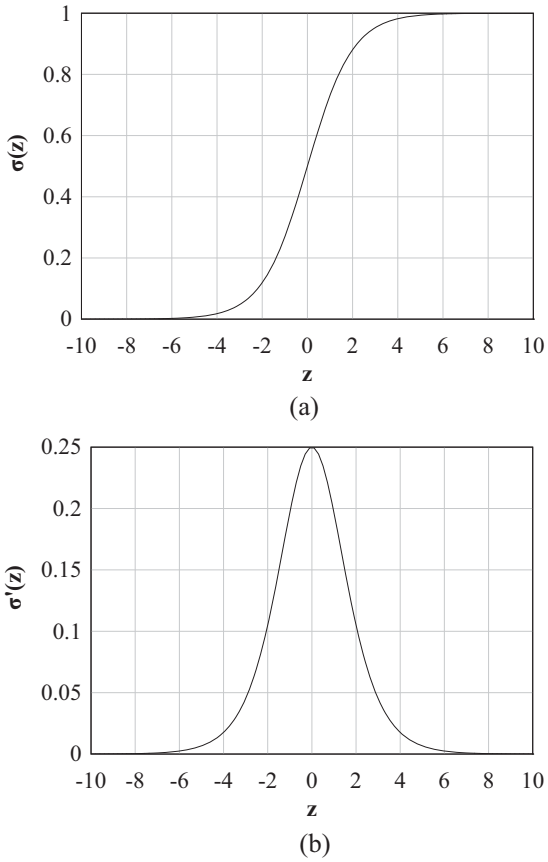

FIGURE 2 The sigmoid function (a) and its derivative (b)

for the last layer L and

$$\delta_k^l = \frac{\partial C_{\text{quadratic}}}{\partial z_k^l} = \sum_j w_{jk}^{l+1}\delta_j^{l+1}\sigma'\left(z_k^l\right) \tag{8}$$

for layer l $(l = 1, 2 \ldots, (L-1))$. Following the SGD-BP algorithm, the weights and biases of C-ANN model (as illustrated in Figure 1) are updated to improve the performance of C-ANN (Goodfellow et al., 2016; Nielsen, 2015).

However, Equation (7) and Equation (8) cause the learning slowdown and vanishing gradient problems of C-ANN as discussed in Section 1. In fact, due to its characteristic, the derivative of sigmoid function gets very small when the sigmoid function (i.e., output activation) is close to zero or one, as depicted in Figure 2. Therefore, the error δ_j^L in Equation (7) might be very small even though C-ANN does not make a good prediction (i.e., $y_j - a_j^L$ is large). However, it is expected that a prediction tool is able to learn faster when it is decisively wrong. This phenomenon is referred to as the learning slowdown problem of C-ANN model (Goodfellow et al., 2016; Nielsen, 2015).

Moreover, the derivative of the sigmoid function varies in range of $[0, 0.25]$, as shown in Figure 2b. Consequently, propagating backward the errors following Equation (8) with the

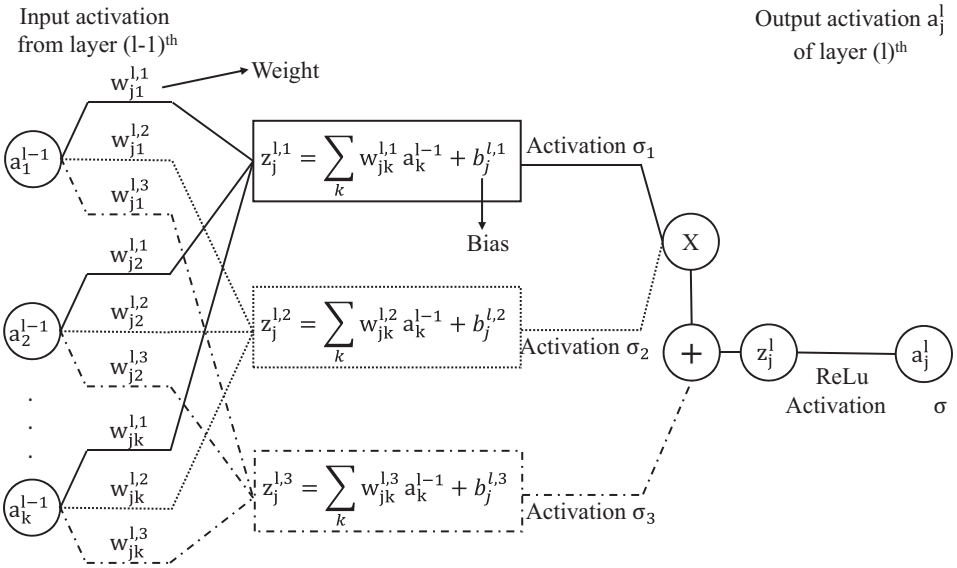

FIGURE 3 The structure of a neuron in the proposed HO-DNN model

sigmoid function results in smaller and smaller errors in the earlier layers. This implies that weights and biases in the earlier layers are adjusted slower, which does not improve the learning process (Goodfellow et al., 2016; Nielsen, 2015). This phenomenon is known as the vanishing gradient problem, one of the main problems of training DNNs with the C-ANN (Schmidhuber, 2015).

3.2 | The development of HO-DNN

The HO-DNN is developed in this section taking into account the limitation of C-ANN model discussed in the previous section. First, the HO-DNN in this study is developed based on a new, high-order neuron, which is motivated by the second-order neuron presented in Fan et al. (2018). The structure of the high-order neuron is presented in Figure 3 in which the weighted input z_j^l is expressed as follows:

$$z_j^l = \sigma_1\left(z_j^{l,1}\right)\sigma_2\left(z_j^{l,2}\right) + \sigma_3\left(z_j^{l,3}\right) \tag{9}$$

where σ_1, σ_2, and σ_3 are the activation functions 1, 2, and 3 in Figure 3, which can be selected to account for nonlinear relationship between the components of the input activations, thereby building up a more complex and abstract model. Despite the fact that the HO-DNN model has triple the parameters as the C-ANN, this does not present a considerable computational difficulty. The new, high-order neuron is more flexible and can cover the second-order neuron proposed by Fan et al. (2018) as a special case when $\sigma_{1,2,3}$ is the linear function. Moreover, the new neuron can take into account higher nonlinear approximations by choosing $\sigma_{1,2,3}$ as any nonlinear functions. It is also worth noting that Fan et al. (2018) used the sigmoid function as an activation (from the weighted input z_j^l to the output activation a_j^l, Figure 3) and the quadratic cost function for the SO-ANN model, which indicates that the SO-ANN model still suffers from the learning slowdown and vanishing gradient problems.

Second, the cross-entropy cost function is used to address the learning slowdown problem in this study as follows:

$$C_{CE} = \sum_j y_j \ln a_j^L + \left(1 - y_j\right)\ln\left(1 - a_j^L\right) \tag{10}$$

Similar to Equation (6), y_j is the actual output corresponding to an input x and a_j^L is the activation of the last (output) layer L when x is input. Although the HO-DNN is fairly complicated with the new neuron and cross-entropy cost function, it is straightforward to implement the SGD-BP for training the model. Indeed, following the SGD-BP algorithm and using the chain rule, the error for the last layer L in the HO-DNN is given as follows:

$$\delta_j^L = \frac{\partial C_{CE}}{\partial z_j^L} = \left(y_j - a_j^L\right) \tag{11}$$

Equation (11) shows that the rate at which the HO-DNN learns (or updates its weights and biases) is solely governed by $(y_j - a_j^L)$ and the effect of derivative $\sigma'(z^L)$ is eliminated, compared to Equation (7) of the C-ANN. Therefore, the HO-DNN directly learns from the error between its prediction and actual output. Hence, the cross-entropy cost function can accelerate the training process of the HO-DNN and help the HO-DNN achieve better performance.

The error for the layer lth ($l = 1, 2 \ldots, (L-1)$) is given as follows:

$$\delta_k^l = \sum_j \begin{bmatrix} w_{jk}^{l+1,1} \sigma'_1\left(z_j^{l+1,1}\right) \sigma_2\left(z_j^{l+1,2}\right) \\ +w_{jk}^{l+1,2} \sigma'_2\left(z_j^{l+1,2}\right) \sigma_1\left(z_j^{l+1,1}\right) \\ +2w_{jk}^{l+1,3} \sigma\left(z_k^l\right) \sigma'_3\left(z_j^{l+1,3}\right) \end{bmatrix} \delta_j^{l+1} \sigma'\left(z_k^l\right) \tag{12}$$

The detailed derivation of Equation (12) is given in Appendix A.

Finally, to overcome the vanishing gradient problem, the ReLU activation function is used in the HO-DNN as depicted in Figure 3. The ReLU activation is given as follows:

$$\sigma(z) = \max(0, z) \tag{13}$$

Although the ReLU activation looks simple and linear, the ReLU is genuinely a nonlinear approximation. In fact, the ReLU activation is prevalent in deep learning researches due to the advantage of its derivative:

$$\sigma'(z) = \begin{cases} 0 & \text{if } z \leq 0 \\ 1 & \text{if } z > 0 \end{cases} \tag{14}$$

As mentioned in Section 3.1, the SGD-BP algorithm works by propagating backward the errors from the last layer L to earlier layers $(L-1), \ldots, 2, 1$ and the range of $[0, 0.25]$ of the derivative of sigmoid activation creates the vanishing gradient problem. As shown in Equation (14), the derivative of ReLU is either one or zero, which alleviates the vanishing gradient problem. It is worth mentioning that the ReLU still has its problem, a so-called dying ReLU problem. The dying ReLU problem occurs when a neuron is inactive and no longer useful during training process (Goodfellow et al., 2016). The dying ReLU activation can be solved by the leaky ReLU activation (Karpathy, 2018). However, it is found that the ReLU activation performs effectively in this study. Therefore, the ReLU is used in this article for the development of HO-DNN. The activations σ_1, σ_2, and σ_3 (Figure 3) are chosen as the linear function. Experimentally, it will be demonstrated that this provides the best prediction of the compressive strength of foamed concrete and high-performance concrete in this study. However, it is believed that different applications might require different selection of activations in the HO-DNN. Therefore, it is important to have the general framework to assure the versatility of the HO-DNN. It is important to note that the sigmoid function is used at the output layer because of an intrinsic issue of using the ReLU activation with the cross-entropy cost function (Nielsen, 2015).

Following the SGD-BP algorithm (Nielsen, 2015), weights and biases of the HO-DNN model are updated as follows:

$$\begin{aligned} w_{jk}^{l,i} &\rightarrow w_{jk}^{l,i} - \eta \frac{\partial C_{CE}}{\partial w_{jk}^{l,i}} \quad \text{for } i = 1, 2, 3 \\ b_j^{l,i} &\rightarrow b_j^{l,i} - \eta \frac{\partial C_{CE}}{\partial b_j^{l,i}} \quad \text{for } i = 1, 2, 3 \end{aligned} \tag{15}$$

where η is a learning rate, which is determined in Section 5; $\frac{\partial C_{CE}}{\partial w_{jk}^{l,i}}$ and $\frac{\partial C_{CE}}{\partial b_j^{l,i}}$ are given as follows:

$$\frac{\partial C_{CE}}{\partial b_j^{l,1}} = \delta_j^l \sigma'_1\left(z_j^{l,1}\right) \sigma_2\left(z_j^{l,2}\right) \tag{16a}$$

$$\frac{\partial C_{CE}}{\partial b_j^{l,2}} = \delta_j^l \sigma_1\left(z_j^{l,1}\right) \sigma'_2\left(z_j^{l,2}\right) \tag{16b}$$

$$\frac{\partial C_{CE}}{\partial b_j^{l,3}} = \delta_j^l \sigma'_3\left(z_j^{l,3}\right) \tag{16c}$$

$$\frac{\partial C_{CE}}{\partial w_{jk}^{l,1}} = \delta_j^l \sigma'_1\left(z_j^{l,1}\right) \sigma_2\left(z_j^{l,2}\right) a_k^{l-1} \tag{16d}$$

$$\frac{\partial C_{CE}}{\partial w_{jk}^{l,2}} = \delta_j^l \sigma_1\left(z_j^{l,1}\right) \sigma'_2\left(z_j^{l,2}\right) a_k^{l-1} \tag{16e}$$

$$\frac{\partial C_{CE}}{\partial w_{jk}^{l,3}} = \delta_j^l \sigma'_3\left(z_j^{l,3}\right) \left(a_k^{l-1}\right)^2 \tag{16f}$$

The detailed derivation of Equation (16) is given in Appendix A.

The developed HO-DNN is implemented in the Python programming language and can be found in Appendix B. The pseudocode of implementation is presented in Algorithm 1. It is worth noting that at the beginning of the algorithm, the weights and biases are initialized at each layer, normally by Gaussian distribution with a mean of zero and a standard deviation of one. However, this strategy of initialization might lead to the saturation of neurons as discussed in Bengio (2012) and Nielsen (2015). Therefore, in this article, the weights and biases of a layer are initialized by a Gaussian distribution with a mean of zero and a standard deviation of $\frac{1}{\sqrt{N}}$ (N is the number of neurons of the layer) to alleviate the saturation of neurons (Bengio, 2012). In Algorithm 1, when all the training data are used, it is said that the training process completes an epoch e and starts over with a new epoch. When the predefined *max_epochs* is reached, the training process of HO-DNN is completed.

Algorithm 1 The pseudo code of HO-DNN

Begin

Input: Training dataset X

Initialise weights $w_{jk}^{l,i}$ and biases $b_j^{l,i}$ $(i = 1, 2, 3)$

While $e \leq max\_epochs$ **do**

For each data x in X **do**

Calculate z_j^l ▷ Using Equation (9)

Calculate $a_j^l = \sigma(z_j^l)$ ▷ Using ReLU activation Equation (13)

Calculate the error δ_j^L of the last layer L ▷ Using Equation (11)

Calculate the error δ_j^l of the earlier layers l $(l = 1, 2 \ldots, (L-1))$ ▷ Using Equation (12)

Update the weights $w_{jk}^{l,i}$ and biases $b_j^{l,i}$ $(i = 1, 2, 3)$ ▷ Using Equation (15) and Equation (16)

end for

Evaluate the cross-entropy cost of HO-DNN at epoch e ▷ Using Equation (10)

Evaluate the performance of HO-DNN at epoch e ▷ Using Equation (18)

$e = e + 1$

end while

Output: Trained HO-DNN model

End

4 | DATA SET AND PERFORMANCE INDICATOR

4.1 | Data collection

The HO-DNN developed in the previous section is used to predict the compressive strength of foamed concrete through a given data set. The data set of foamed concrete (Data set 1) consists of 177 testing results for different mixtures (density, water-to-cement [w/c] ratio, and sand-to-cement [s/c] ratio). The samples of the Data set 1 were consistently made up of ordinary Portland cement, water, sand, and preformed foams, curing time of 28 days (Abd & Abd, 2017; Asadzadeh & Khoshbayan, 2018; Jones & McCarthy, 2005; Kiani et al., 2016; Pan, Hiromi, & Wee, 2007). The range of density, w/c ratio, and s/c ratio were $[430 - 2{,}009]$ kg/m^3, $[0.26 - 0.83]$, and $[0 - 4.3]$, respectively. After developed and validated by the Data set 1, the trained HO-DNN is supposed to be capable of predicting the foamed concrete strength correctly. Therefore, the trained HO-DNN was then exposed to a new data set (Data set 1A), which is completely different from the Data set 1. The Data set 1A consisting of 34 samples was prepared in the laboratory, having a density and w/c ratio in the range of $[444 - 2{,}066]$ kg/m^3 and $[0.3 - 0.7]$, respectively. It is worth noting that the HO-DNN is trained in the range of $[430 - 2{,}009]$ for density, while the Data set 1A has the density in the range of $[444 - 2{,}066]$, outside of the training range. It is accepted that it is not recommended to use the HO-DNN for such extrapolation. However, for the Data set 1A, it is a very near extrapolation (i.e., the Data set 1A slightly exceeds the training region). Indeed, after normalization by Equation (17), the training region is in the range of $[0 - 1]$ for density and the Data set 1A is in the range of $[0.009 - 1.036]$ for the density. Therefore, it is assumed that the effect of such near extrapolation is negligible in this article. For the Data set 1A, general-purpose ordinary Portland cement and a commercial foaming agent (Isochem S/X from Isoltech, Italy) are used to fabricate three foamed concrete groups: high, medium, and low density. The cubic samples of $50 \times 50 \times 50$ mm in size are cured in sealed plastic bags at ambient temperature for 28 days. The uniaxial compressive strength of foamed concrete is measured using the INSTRON 5569A machine. The displacement-controlled test is conducted at a velocity of 0.03 mm/s to obtain the compressive strength. The purpose of the Data set 1A is to show that the HO-DNN can obtain the reliable prediction of a new Data set that the model has never been exposed, thereby helping the design of foamed concrete mixture.

Furthermore, to demonstrate the efficacy and versatility of the proposed HO-DNN model for different engineering applications, the HO-DNN is validated through the other data set of high-performance concrete (Data set 2). The Data set 2 is retrieved from the ML benchmark repository at the University of California, Irvine, and consists of 1,133 testing results of high-performance concrete with different mixtures of cement, slag, fly ash, water, superplasticizer, fine and coarse aggregate, and age of testing (Yeh, 1998). The Data set 2 was originally provided by Yeh (1998) and subsequently contributed by

other researchers (Yeh, 2006). The Data set 2 was extensively used in the literature (Bui et al., 2018; Chou, Tsai, Pham, & Lu, 2014; Chou & Pham, 2013; Mousavi, Aminian, Gandomi, Alavi, & Bolandi, 2012; Rafiei et al., 2017a, 2017b) and the information of the Data set 2 was detailed in these references. It is noted that the foamed concrete (and high-performance concrete for the Data set 2) might exhibit a variation of compressive strength due to the uncertainty of the preparation and testing of concrete material (Gribniak, Mang, Kupliauskas, & Kaklauskas, 2015; Gribniak, Mang, Kupliauskas, Kaklauskas, & Juozapaitis, 2016). However, the main objective of this study is to develop the new HO-DNN and demonstrate its efficiency and versatility. Therefore, it is assumed that the uncertainty of data is neglected in this study. It is known that this assumption is commonly accepted in the literature (Abd & Abd, 2017; Chou & Pham, 2013; Rafiei et al., 2017a, 2017b; Yaseen et al., 2018). Investigations on the influence of uncertainty on DNN models can be found in the literature (Antoniades et al., 2018; Gal, 2016; Koziarski & Cyganek, 2017).

Finally, to avoid the magnitude difference between inputs (e.g., density: 430–2,009 kg/m^3; w/c ratio: 0.26–0.83), all data were normalized to the range of [0, 1] using the following equation:

$$x_{\text{norm}} = \frac{x - x_{\min}}{x_{\max} - x_{\min}} \tag{17}$$

This data normalization is crucial to avoid numerical difficulties in the calculation because of the magnitude difference between input values (Chou & Pham, 2013). The Data sets 1, 1A, and 2 are available publicly in Appendix B.

4.2 | Performance indicators

In this study, the accuracy of the proposed HO-DNN was assessed by comparing the actual (y) and predicted (y^{pre}) compressive strength for the Data sets 1, 1A, and 2. The correlation coefficient (R), root mean square error (RMSE), mean absolute error (MAE), relative RMSE (RRMSE), and relative MAE (RMAE) were used as performance indicators, as follows:

$$R = \frac{\sum_{i=1}^{n}\left(y_i - \bar{y}\right)\left(y_i^{\text{pre}} - \bar{y}^{\text{pre}}\right)}{\sqrt{\sum_{i=1}^{n}\left(y_i - \bar{y}\right)^2 \sum_{i=1}^{n}\left(y_i^{\text{pre}} - \bar{y}^{\text{pre}}\right)^2}} \tag{18a}$$

$$RMSE = \sqrt{\frac{1}{n}\sum_{i=1}^{n}\left(y_i - y_i^{\text{pre}}\right)^2} \tag{18b}$$

$$MAE = \frac{1}{n}\sum_{i=1}^{n}\left|y_i - y_i^{\text{pre}}\right| \tag{18c}$$

$$RRMSE = \frac{RMSE}{\bar{y}} \times 100 \tag{18d}$$

$$RMAE = \frac{MAE}{\bar{y}} \times 100 \tag{18e}$$

where n is the number of data; and $\bar{y}$ and $\bar{y}^{\text{pre}}$ are the mean actual and predicted value, respectively.

The correlation coefficient R is used to quantify the degree of linear dependence between the actual value and the predicted value (Yaseen et al., 2018). When R is close to zero, it means that there is no evidence of any relationship between the actual and predicted value, while when R is close to one, we are close to a perfect fit between the actual and predicted value (Chou & Pham, 2013). However, the result of R is not sufficient to evaluate the accuracy of a model because it does not significantly change when y_i^{pre} is multiplied by a constant. Therefore, RMSE and MAE are the additional indicators to check the goodness-of-fit (in MPa units) of the ANN models. Moreover, RRMSE and RMAE are employed to investigate the percentage deviation of the actual and predicted data. In general, the higher value of R and the lower value of RMSE, MAE, RRMSE, and RMAE result in a decrease of errors between the actual and predicted value, and thereby indicate the accuracy of models.

5 | RESULTS AND DISCUSSION

5.1 | Comparative study

This section presents the application of the developed HO-DNN for the prediction of foamed concrete strength. To compare the performance of the HO-DNN, the C-ANN presented in Section 3.1 and the SO-ANN, which was presented in Fan et al. (2018), are used. The description of the C-ANN, SO-ANN, and HO-DNN is presented in Table 1. It is noted that the C-ANN with three and six hidden layers and the SO-ANN and HO-DNN with one and two hidden layers have the same number of weights and biases, respectively. To construct and validate the C-ANN, SO-ANN, and HO-DNN, the data of the Data set 1 are randomly split into training data (80%), validating data (10%), and testing data (10%). To avoid the effect of randomness of data, the same training, validating, and testing data were used for the three models in this study. That means three models display the same level of randomness and uncertainty of data. Therefore, the comparison of three models is valid and informative. In this study, the training process is completed when the *max_epochs* is equal to 2,000 (Algorithm 1).

The effects of learning rate η and the number of neurons of hidden layer are first investigated for the C-ANN model by the validating data of Data set 1. Figure 4a shows the variation of

TABLE 1 The description of the C-ANN, SO-ANN, and DO-DNN model

Model	Number of hidden layers	Number of neurons per layer	Learning rate η	Type of neurons	Activation function	Cost function
C-ANN	1, 3, 6	30	0.01	Linear	Sigmoid	Quadratic
SO-ANN	1, 2	30	0.01	Second order	Sigmoid	Quadratic
HO-DNN	1, 2	30	0.01	High order	ReLU	Cross-entropy

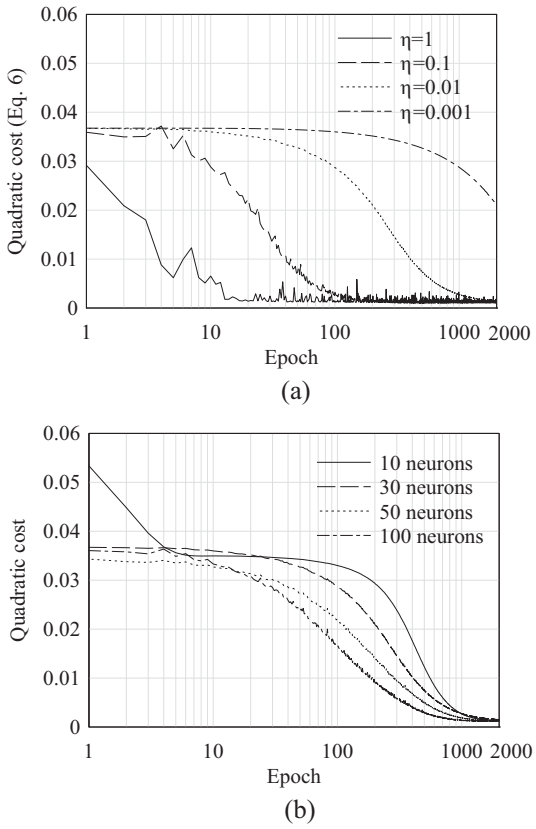

FIGURE 4 The effects of learning rate η (a) and the number of neurons of hidden layer (b) on the performance of C-ANN. The quadratic cost is evaluated using Equation (6) for the validating data of the Data set 1

the quadratic cost Equation (6) for validating data during the training process. The C-ANN model is used with one hidden layer, 30 neurons in the hidden layer, and different learning rate $\eta = 1, 0.1, 0.01, 0.001$. Apparently, a large value of the learning rate ($\eta = 1, 0.1$) increases the resultant noise. This is attributed to the fact that the model learns too fast and may overshoot an expected minimum. On the contrary, this oscillation of the result can be alleviated by using a small learning rate ($\eta = 0.01, 0.001$). However, a very small learning rate ($\eta = 0.001$) slows down the learning process, increasing the training time until the solution process converges. Figure 4a shows the learning rate of 0.01 is appropriate for the C-ANN in this study. The effect of the number of neurons of hidden layer is presented in Figure 4b for the C-ANN with one hidden layer and the learning rate of 0.01. Figure 4b shows that the number of neurons of hidden layer has negligible effect on the C-ANN, in which four cases are converged. It is also observed in Figure 4b that the 50- and 100-neuron case leads to oscillating results. Therefore, the number of neurons of hidden layers is 30 for the C-ANN as presented in Table 1. Moreover, the variation of the quadratic cost (Figure 4) for validating data during the training process shows that overfitting problem does not occur in this study. Because the cost of validating data decreases gradually during the training process (Marsland, 2015). In the same way, the learning rate and number of neurons of the SO-ANN and HO-DNN are 0.01 and 30, respectively, as given in Table 1. It is noted that the same learning rate and number of neurons assure the fair comparison of C-ANN, SO-ANN, and HO-DNN models.

Table 2 shows the comparison of the C-ANN, SO-ANN, and HO-DNN models with different number of hidden layers (N_layers) for the validating data of the Data set 1. As aforementioned, the C-ANN (N_layers= 3, 6), the SO-ANN (N_layers= 1, 2), and the HO-DNN (N_layers= 1, 2) have the same number of weights of biases, respectively. It is shown that the HO-DNN (N_layers= 1, 2) outperforms the SO-ANN due to the advantages of cross-entropy cost and ReLU activation functions. Moreover, the HO-DNN (N_layers= 2) achieves the lowest RMSE and MAE (1.65 and 1.17 MPa, respectively), which exhibits approximately 36% and 48% improvement compared with the C-ANN (N_layers= 1). Table 2 also demonstrates the vanishing gradient problem of the C-ANN and SO-ANN. In fact, adding more hidden layers does not improve, but genuinely degrades the performances of C-ANN model as presented for the cases of N_layers= 3, 6 in Table 2. The same phenomenon can be observed for the SO-ANN in Table 2, in which the performances of SO-ANN with two hidden layers are worse than those of one hidden layer. On the contrary, the proposed HO-DNN genuinely improves its performances when adding more hidden layers as shown in Table 2. That is why the present approach is named as high-order "deep" neural network, while the other models are conventional and SO-ANN. It is remarkable that the HO-DNN with two hidden layers can break the 0.9900 barrier of the correlation coefficient R that is not possible with the C-ANN and SO-ANN.

After the architecture (e.g., number of hidden layer, number of neurons, and learning rate) of the models is determined using the validating data, the C-ANN (N_layers= 1), the SO-ANN (N_layers= 1), and the HO-DNN (N_layers= 2)

TABLE 2 The comparison of the C-ANN, SO-ANN, and HO-DNN models with different number of hidden layers (N_layers) for the validating data of the Data set 1

Model	N_layers	*R*	RMSE (MPa)	MAE (MPa)	RMMSE (%)	RMAE (%)
C-ANN	1	0.9828	2.58	2.25	9.45	8.23
C-ANN	3	0.9639	4.52	3.83	16.55	14.04
		(−1.92)	(−75.08)	(−70.61)	(−75.13)	(−70.60)
C-ANN	6	0.7177	12.79	11.36	46.82	41.59
		(−26.97)	(−395.43)	(−405.39)	(−395.45)	(−405.35)
SO-ANN	1	0.9865	2.15	1.77	7.87	6.49
		(0.38)	(16.75)	(21.16)	(16.72)	(21.14)
SO-ANN	2	0.9854	2.18	1.88	7.98	6.87
		(0.26)	(15.59)	(16.48)	(15.56)	(16.52)
HO-DNN*	1	0.9877	2.15	1.67	7.87	6.11
		(0.50)	(16.76)	(25.80)	(16.72)	(25.76)
HO-DNN*	2	0.9921	1.65	1.17	6.06	4.29
		(0.95)	(35.91)	(47.89)	(35.87)	(47.87)

Values in parentheses indicate the improvement (%) compared to the C-ANN, N_layers= 1. * indicates that the performances are genuinely improved for a deep model.

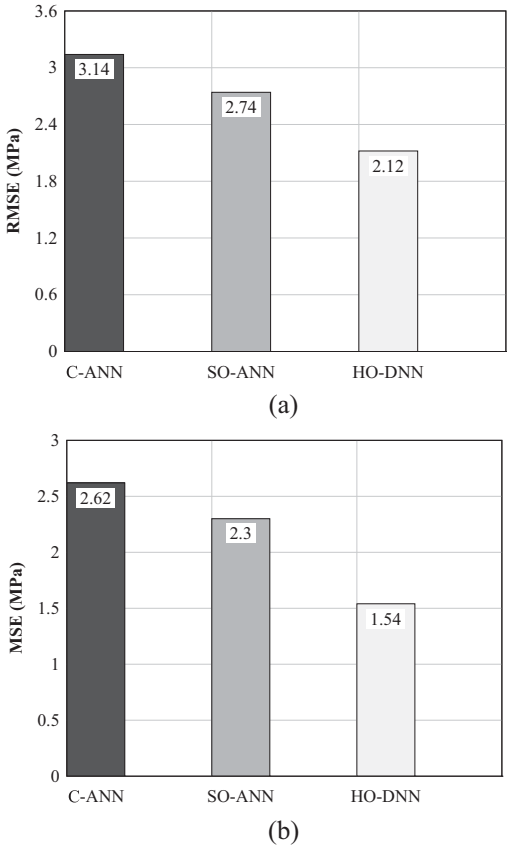

FIGURE 5 The comparison of the C-ANN, SO-ANN, and HO-DNN for the testing data of the Data set 1: (a) root mean square error (RMSE) (Equation 18b) and (b) mean absolute error (MAE) (Equation 18c)

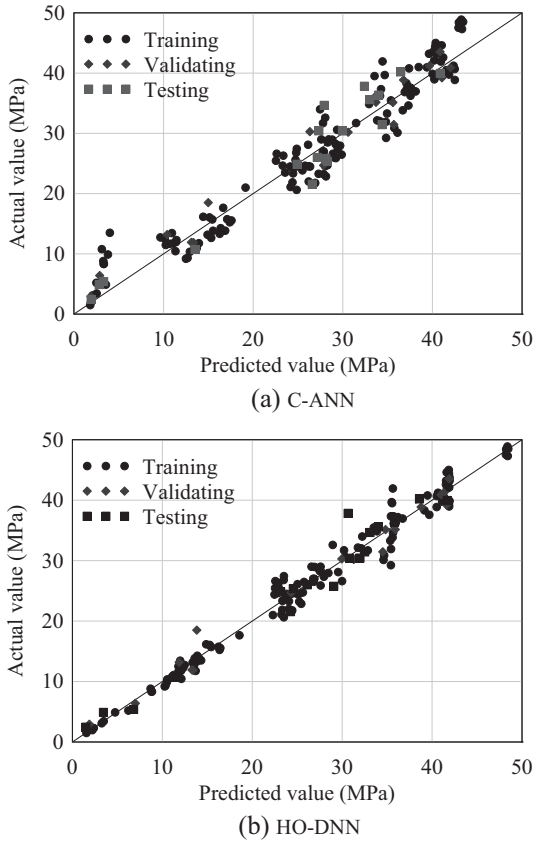

FIGURE 6 The correlation between the actual and predicted foamed concrete strength of the Data set 1 using the C-ANN and HO-DNN models

are validated for the testing data of the Data set 1 in Figure 5. It is shown that the HO-DNN is better than the C-ANN and SO-ANN in the prediction of foamed concrete strength for the testing data of Data set 1. In fact, the HO-DNN produces the smallest RMSE and MAE (2.12 and 1.54 MPa, respectively). On the other hand, the C-ANN provides the prediction at a lowest level of accuracy with the highest RMSE and MAE (3.14 and 2.62 MPa, respectively). Figure 6 shows the

TABLE 3 The comparison of performance and improvement rates of the HO-DNN for the testing data of the Data set 2

	Performance			Improved by HO-DNN (%)		
Model	***R***	**RMSE (MPa)**	**MAE (MPa)**	***R***	**RMSE**	**MAE**
GEP+	0.91	–	5.20	6.59*	–	45.19*
M-GGP+	0.90	7.31	5.48	7.78*	44.60*	47.99*
ANN-SVR+	0.94	6.17	4.24	3.19	34.36*	32.78*
SFA-LSSVR+	0.94	5.62	3.86	3.19	27.94	26.17
MFA-ANN+	0.95	4.85	3.41	2.11	16.49	16.42
C-ANN (present)	0.90	7.17	5.59	7.78*	43.51*	49.02*
SO-ANN (present)	0.93	5.82	4.50	4.30	30.41*	36.67*
HO-DNN (present)	0.97	4.05	2.85	–	–	–

+indicates the results are obtained from the literature. *indicates significant improvements by HO-DNN (≥ 5% for *R*, ≥ 30% for RMSE and MAE).

correlation between the actual and predicted compressive strength of foamed concrete for the training, validating, and testing data of the Data set 1 using the C-ANN (N_layers= 1) and HO-DNN (N_layers= 2). It is obvious that the HO-DNN achieves the most reliable prediction as shown in Figure 6 as well as Table 2 and Figure 5. This can be attributed to the use of high-order neurons in the HO-DNN, incorporating with the ReLU and cross-entropy cost functions. In fact, it is known that the compressive strength of foamed concrete is a highly nonlinear function of its density and constituents (Ngo et al., 2017; Nguyen et al., 2017; Nguyen et al., 2018). The high-order neurons enable the HO-DNN to account for the higher order relationship between neurons rather than the linear inner product of the C-ANN, while the ReLU and cross-entropy cost function improve the training process and enable a genuinely DNN model. As a result, the HO-DNN model outperforms the C-ANN and SO-ANN models in predicting the foamed concrete strength of the Data set 1.

To demonstrate the efficacy and versatility of the proposed HO-DNN method for different engineering applications, the HO-DNN, SO-ANN, and C-ANN are tested through the Data set 2 of the compressive strength of high-performance concrete. The architecture of HO-DNN, SO-ANN, and C-ANN is identical with the previous example of the Data set 1. The Data set 2 is randomly split into training data (90%) and testing data (10%) (Bui et al., 2018; Chou & Pham, 2013). Table 3 shows the performance of the proposed HO-DNN in the prediction of the Data set 2. The performance of the HO-DNN is compared with the C-ANN, SO-ANN, and other ML methods reported in the literature including gene expression programming (GEP) (Mousavi et al., 2012), multigene genetic programming (M-GGP) (Gandomi, Alavi, Shadmehri, & Sahab, 2013), ensemble model artificial neural network-support vector regression (ANN-SVR) (Chou & Pham, 2013), smart firefly algorithm-based least squares SVR (SFA-LSSVR) (Chou, Chong, & Bui, 2016), and modified firefly algorithm-based ANN (MFA-ANN) (Bui et al., 2018). Table 3 shows that the proposed HO-DNN obtains the best prediction for the Data set 2 with the correlation coefficient *R* of 0.97, the RMSE of 4.05 MPa, and the MAE of 2.85 MPa, compared to other methods. In general, the RMSE and MAE of the HO-DNN are about 17%–45% and 16%–49%, respectively, better than those of other methods. While the results of SO-ANN are comparable with those of GEP (Mousavi et al., 2012) and M-GGP (Gandomi et al., 2013) methods. Figure 7 depicts the correlation between the actual and predicted strength of the Data set 2 using the HO-DNN and C-ANN models. It is

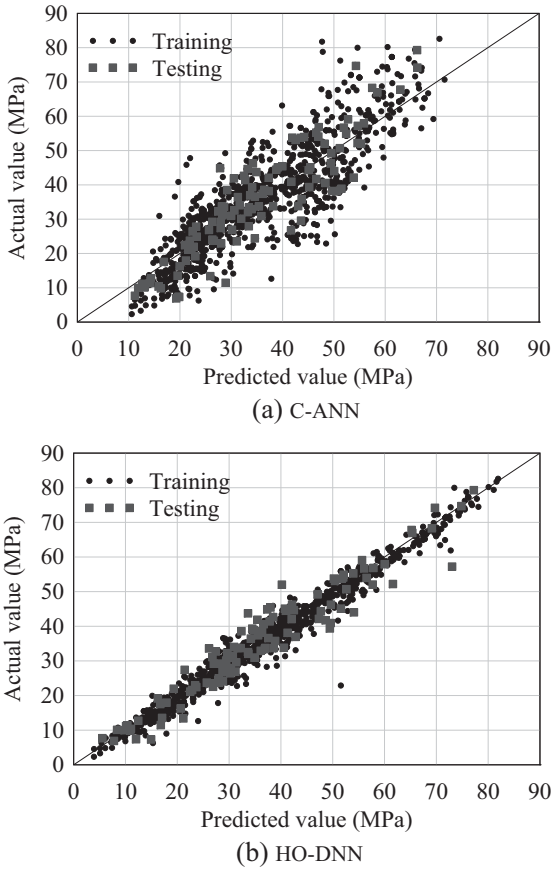

(a) C-ANN

(b) HO-DNN

FIGURE 7 The correlation between the actual and predicted compressive strength of the Data set 2 using the C-ANN and HO-DNN models

TABLE 4 The comparison of C-ANN, SO-ANN, HO-DNN, and two empirical equations in predicting the compressive strength of the data set 1A

Model	*R*	RMSE (MPa)	MAE (MPa)	RMMSE (%)	RMAE (%)
Hoff	0.9911	4.89	2.559	31.58	16.48
Nambiar	0.9913	3.17	1.75	20.46	11.31
C-ANN	0.9937	2.11	1.39	13.66	8.96
SO-ANN	0.9951	1.90	1.29	12.26	8.35
HO-DNN	0.9978	1.30	0.91	8.38	5.89

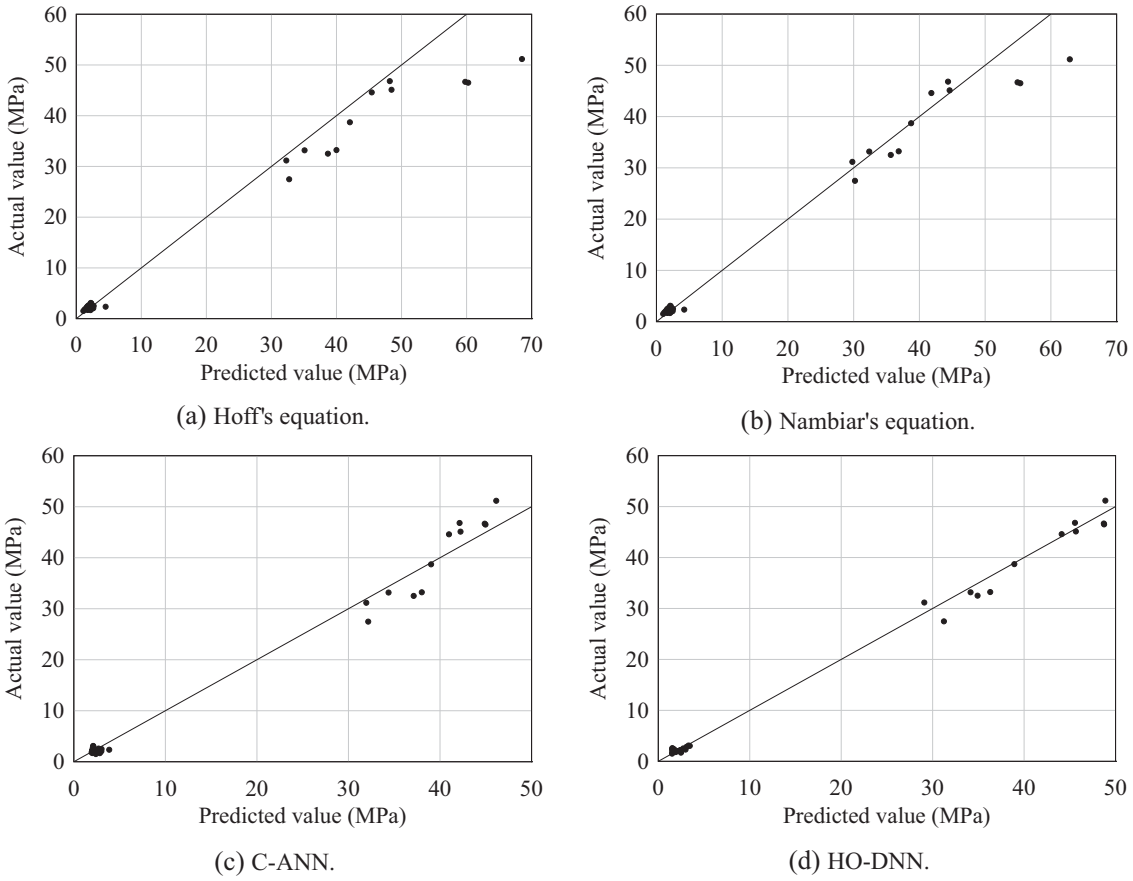

FIGURE 8 The correlation between the actual and predicted compressive strength of the Data set 1A

observed that by using the HO-DNN, the predicted strengths are closer to the actual strength, compared to the C-ANN model. The obtained results for the Data set 1 and Data set 2 show that the proposed HO-DNN provides a reliable and versatile prediction tool for engineering applications.

5.2 | Accuracy of the proposed HO-DNN on the new Data set 1A

In the previous section, the proposed HO-DNN was validated through the Data set 1 and Data set 2 from the literature. It was shown that the HO-DNN can deliver the best performance in predicting the foamed concrete strength of the Data set 1. To achieve a higher degree of confidence and demonstrate that the proposed HO-DNN is genuinely capable of aiding researchers and engineers in the practical design of foamed concrete, the trained HO-DNN model was tested with the Data set 1A for foamed concrete in this section. The obtained results are compared with two empirical equations presented in Section 2, the Hoff's equation (Equation 1) and Nambiar's equation (Equation 2). It is accepted that the Hoff's and Nambiar's equations are commonly used to predict the compressive strength of foamed concrete in the mixture design of foamed concrete. The Hoff's equation (Equation 1) is used with $\sigma_0 = 115$ MPa, and $b = 2.7$ as given by Hoff (1972) and the Nambiar's equation is used with $\sigma_0 = 105.14$ MPa, and $b = 2.68$ as given by Nambiar and Ramamurthy (2008). Table 4 presents the comparison of the trained

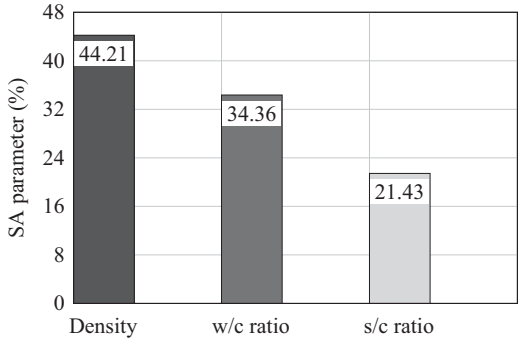

FIGURE 9 The sensitivity analysis for the compressive strength of foamed concrete

C-ANN, trained SO-ANN, trained HO-DNN models, and two empirical equations in the prediction of the Data set 1A. The correlation between the actual and predicted strength of the Data set 1A is depicted in Figure 8 using the C-ANN, HO-DNN, and Hoff's and Nambia's equations. Due to the small number of data in the Data set 1A (34 data), it is easy for all methods (Hoff's, Nambiar's, C-ANN, SO-ANN, and HO-DNN) to obtain a high value for the correlation coefficient R (Table 4). However, the relative errors (RRMSE and RMAE) of Hoff's, Nambiar's, C-ANN, and SO-ANN methods are higher than 10%, indicating a low level of prediction accuracy. It can be observed in Figure 8 that Hoff and Nambiar (Figures 8a and 8b) equations can provide the good prediction of low-strength values group but not high-strength values group. On the contrary, the HO-DNN model is able to predict accurately the compressive strength of the Data set 1A with an acceptable relative error (less than 8.38% in Table 4). Based on the examples of the Data set 1 and Data set 1A, one can conclude that the proposed HO-DNN provides a reliable and accurate tool to predict the compressive strength of foamed concrete. Achieving the RRMSE of 8.38% and the RMAE of 5.89% for the Data set 1A, the proposed HO-DNN model can realistically benefit the design of foamed concrete by reducing the laboratory work required.

5.3 | Sensitivity analysis

With the reliable HO-DNN model presented in the previous sections, an SA can be conducted to examine the effect of density, w/c ratio, and s/c ratio on the compressive strength of foamed concrete. To conduct the sensitivity study, the compressive strength of foamed concrete was determined by changing one input variable, while other variables are kept constant at the average values (Kiani et al., 2016). For instance, to examine the effect of density, density is varied from 430 to 2,009 kg/m^3 and the w/c and s/c ratios were held constant at 0.405 and 1.167, respectively. Once the data for the SA study were created, the data were fed into the trained HO-DNN model to obtain the compressive strength. For each input variable, a corresponding SA parameter can be simply evaluated as follows (Gandomi, Tabatabaei, Moradian, Radfar, & Alavi, 2011):

$$I_i = f_{\max}(x_i) - f_{\min}(x_i) \tag{19a}$$

$$SA_i = \frac{I_i}{\sum_i I_i} \times 100 \tag{19b}$$

in which $f_{\max}(x_i)$ and $f_{\min}(x_i)$ are the maximum and minimum predicted strength corresponding to the input variable x_i, while other input variables are kept constant at their average values. Figure 9 shows the SA results of the compressive strength of foamed concrete with respect to density, w/c ratio, and s/c ratio. As shown in Figure 9, the compressive strength of foamed concrete is strongly influenced by its density that has the SA parameter of about 44%. This can be attributed to the fact that air voids in foamed concrete, which reduce density, collapse, and coalesce into macrocracks inside materials under mechanical load, leading to a decrease in the compressive strength (Hajimohammadi, Ngo, & Mendis, 2018; Nguyen et al., 2018). Figure 9 also shows that the w/c ratio is the second important parameter with an SA parameter of about 34.5%, followed by the s/c ratio with an SA parameter of about 21.5%. In fact, the similar observation can also be found in the literature (Kiani et al., 2016; Ramamurthy, Nambiar, & Ranjani, 2009).

6 | CONCLUSIONS

In this article, a deep, high-order neural network (HO-DNN) was presented for predicting the compressive strength of foamed concrete (Data set 1, Data set 1A) and high-performance concrete (Data set 2). Particularly, this study proposed a new, high-order neuron for the deep neural network model to account for nonlinear relationship between input activations at layers. Furthermore, the cross-entropy cost and ReLU activation functions were used to develop the HO-DNN to improve the performances and alleviate the vanishing gradient problem when training a deep neural network model. The accuracy of the proposed HO-DNN in predicting the compressive strength of the Data set 1 and Data set 2 is obtained and compared with a C-ANN, an SO-ANN proposed by Fan et al. (2018), and other methods from previous studies (for Data set 2).

The higher order neuron, cross-entropy cost, and ReLU activation functions significantly improved the performances of the HO-DNN, compared to the C-ANN and SO-ANN. The cross-entropy cost function helped the proposed HO-DNN to learn quickly and more accurately. The ReLU activation function alleviates the vanishing gradient problem and genuinely improved the performance of the HO-DNN when

training multiple hidden layers. For the Data set 1, the HO-DNN outperformed the C-ANN and SO-ANN in the prediction of foamed concrete strength with the remarkable improvements of 36% (RMSE) and 48% (MAE) compared to the C-ANN model. Notably, the HO-DNN model was able to break the 0.99 barrier of the correlation coefficient *R* that was not possible with the C-ANN and SO-ANN. For the Data set 2, the developed HO-DNN was better than other methods presented in the previous studies. The improvement rates of RMSE and MAE were approximately 50% for GEP method, M-GGP method, and C-ANN method.

To further demonstrate the accuracy of the HO-DNN in the prediction of foamed concrete strength, the trained HO-DNN model (by the Data set 1) was validated through the Data set 1A obtained from the laboratory. The comparison between the trained HO-DNN with two empirical equations showed that the HO-DNN can predict the foamed concrete strength with a high level of accuracy. Having the reliable HO-DNN model, an SA was conducted to investigate the effects of the input variables on the compressive strength of foamed concrete. It was shown that density is the most important factor affecting the compressive strength of foamed concrete with an SA parameter of about 44.2%, followed by w/c ratio (34.4%) and s/c ratio (21.4%).

While the proposed HO-DNN model was used to predict the compressive strength of concrete material in this study, it can be used to estimate other properties of concrete such as thermal conductivity, flexural strength. Therefore, the proposed framework can support researcher and engineers in mixture design optimization of concrete. Moreover, it is desirable to investigate the application of the HO-DNN for different engineering problems in future studies.

ACKNOWLEDGMENTS

The authors would like to thank the Editor and the five anonymous reviewers for their constructive comments and valuable suggestions to improve the quality of the article. The first author would like to thank the University of Melbourne for offering the Melbourne Research Scholarship. The authors would like to acknowledge the support of the ARC Centre for Advanced Manufacturing of Prefabricated Housing (ARC IC150100023).

REFERENCES

Abd, A. M., & Abd, S. M. (2017). Modelling the strength of lightweight foamed concrete using support vector machine (SVM). *Case Studies in Construction Materials*, *6*, 8–15.

Adeli, H. (2001). Neural networks in civil engineering: 1989–2000. *Computer-Aided Civil and Infrastructure Engineering*, *16*(2), 126–142.

Adeli, H., & Panakkat, A. (2009). A probabilistic neural network for earthquake magnitude prediction. *Neural Networks*, *22*(7), 1018–1024.

Adeli, H., & Wu, M. (1998). Regularization neural network for construction cost estimation. *Journal of Construction Engineering and Management*, *124*(1), 18–24.

Antoniades, A., Spyrou, L., Martin-Lopez, D., Valentin, A., Alarcon, G., Sanei, S., & Took, C. C. (2018). Deep neural architectures for mapping scalp to intracranial EEG. *International Journal of Neural Systems*, *28*, 1850009.

Asadzadeh, S., & Khoshbayan, S. (2018). Multi-objective optimization of influential factors on production process of foamed concrete using Box-Behnken approach. *Construction and Building Materials*, *170*, 101–110.

Bengio, Y. (2012). Practical recommendations for gradient-based training of deep architectures. In G. Montavon, G. B. Orr, & K. R. Müller (Eds.), *Neural networks: Tricks of the trade. Lecture notes in computer science* (Vol. 7700, pp 437–478). Springer, Berlin, Heidelberg.

Bui, D.-K., Nguyen, T., Chou, J.-S., Nguyen-Xuan, H., & Ngo, T. D. (2018). A modified firefly algorithm-artificial neural network expert system for predicting compressive and tensile strength of high-performance concrete. *Construction and Building Materials*, *180*, 320–333.

Chiew, F. H., Ng, C. K., Chai, K. C., & Tay, K. M. (2017). A fuzzy adaptive resonance theory-based model for mix proportion estimation of high-performance concrete: A fuzzy adaptive resonance theory. *Computer-Aided Civil and Infrastructure Engineering*, *32*(9), 772–786.

Chou, J.-S., Chong, W. K., & Bui, D.-K. (2016). Nature-inspired metaheuristic regression system: programming and implementation for civil engineering applications. *Journal of Computing in Civil Engineering*, *30*(5), 04016007.

Chou, J.-S., & Pham, A.-D. (2013). Enhanced artificial intelligence for ensemble approach to predicting high performance concrete compressive strength. *Construction and Building Materials*, *49*, 554–563.

Chou, J.-S., & Pham, A.-D. (2015). Smart artificial firefly colony algorithm-based support vector regression for enhanced forecasting in civil engineering: Smart artificial firefly colony-based support vector regression. *Computer-Aided Civil and Infrastructure Engineering*, *30*(9), 715–732.

Chou, J.-S., Tsai, C.-F., Pham, A.-D., & Lu, Y.-H. (2014). Machine learning in concrete strength simulations: Multi-nation data analytics. *Construction and Building Materials*, *73*, 771–780.

Dai, H., & Cao, Z. (2017). A wavelet support vector machine-based neural network metamodel for structural reliability assessment. *Computer-Aided Civil and Infrastructure Engineering*, *32*(4), 344–357.

DeRousseau, M. A., Kasprzyk, J. R., & Srubar, W. V. (2018). Computational design optimization of concrete mixtures: A review. *Cement and Concrete Research*, *109*, 42–53.

Dharia, A., & Adeli, H. (2003). Neural network model for rapid forecasting of freeway link travel time. *Engineering Applications of Artificial Intelligence*, *16*(7–8), 607–613.

Fan, F., Cong, W., & Wang, G. (2018). A new type of neurons for machine learning. *International Journal for Numerical Methods in Biomedical Engineering*, *34*(2), e2920.

Gal, Y. (2016). *Uncertainty in deep learning*. Cambridge, U.K.: University of Cambridge.

Gandomi, A. H., Alavi, A. H., Shadmehri, D. M., & Sahab, M. (2013). An empirical model for shear capacity of RC deep beams using genetic-simulated annealing. *Archives of Civil and Mechanical Engineering*, *13*(3), 354–369.

Gandomi, A. H., Tabatabaei, S. M., Moradian, M. H., Radfar, A., & Alavi, A. H. (2011). A new prediction model for the load capacity of castellated steel beams. *Journal of Constructional Steel Research*, *67*(7), 1096–1105.

Gao, Y., & Mosalam, K. M. (2018). Deep transfer learning for image-based structural damage recognition. *Computer-Aided Civil and Infrastructure Engineering*, *33*, 748–768.

García-Ródenas, R., López-García, M. L., & Sánchez-Rico, M. T. (2017). An approach to dynamical classification of daily traffic patterns. *Computer-Aided Civil and Infrastructure Engineering*, *32*(3), 191–212.

Goodfellow, I., Bengio, Y., & Courville, A. (2016). *Deep learning*. Cambridge, MA: MIT Press.

Grande, Z., Castillo, E., Mora, E., & Lo, H. K. (2017). Highway and road probabilistic safety assessment based on Bayesian network models. *Computer-Aided Civil and Infrastructure Engineering*, *32*(5), 379–396.

Gribniak, V., Mang, H. A., Kupliauskas, R., & Kaklauskas, G. (2015). Stochastic tension-stiffening approach for the solution of serviceability problems in reinforced concrete: Constitutive modeling. *Computer-Aided Civil and Infrastructure Engineering*, *30*(9), 684–702.

Gribniak, V., Mang, H. A., Kupliauskas, R., Kaklauskas, G., & Juozapaitis, A. (2016). Stochastic tension-stiffening approach for the solution of serviceability problems in reinforced concrete: Exploration of predictive capacity. *Computer-Aided Civil and Infrastructure Engineering*, *31*(6), 416–431.

Hajimohammadi, A., Ngo, T., & Mendis, P. (2017a). How does aluminium foaming agent impact the geopolymer formation mechanism? *Cement and Concrete Composites*, *80*(Supplement C), 277–286.

Hajimohammadi, A., Ngo, T., & Mendis, P. (2018). Enhancing the strength of pre-made foams for foam concrete applications. *Cement and Concrete Composites*, *87*, 164–171.

Hajimohammadi, A., Ngo, T., Mendis, P., Nguyen, T., Kashani, A., & van Deventer, J. S. J. (2017b). Pore characteristics in one-part mix geopolymers foamed by H2o2: The impact of mix design. *Materials & Design*, *130*(Supplement C), 381–391.

Hajimohammadi, A., Ngo, T., Mendis, P., & Sanjayan, J. (2017c). Regulating the chemical foaming reaction to control the porosity of geopolymer foams. *Materials & Design*, *120*, 255–265.

Hoff, G. C. (1972). Porosity-strength considerations for cellular concrete. *Cement and Concrete Research*, *2*(1), 91–100.

Jones, M., & McCarthy, A. (2005). Preliminary views on the potential of foamed concrete as a structural material. *Magazine of Concrete Research*, *57*(1), 21–31.

Karpathy, A. (2018). Stanford University CS231n: Convolutional Neural Networks for Visual Recognition.

Kiani, B., Gandomi, A. H., Sajedi, S., & Liang, R. Y. (2016). New formulation of compressive strength of performed-foam cellular concrete: An evolutionary approach. *Journal of Materials in Civil Engineering*, *28*(10), 04016092.

Koziarski, M., & Cyganek, B. (2017). Image recognition with deep neural networks in presence of noise–dealing with and taking advantage of distortions. *Integrated Computer-Aided Engineering*, *24*(4), 337–349.

Ley, C., & Bordas, S. P. A. (2018). What makes data science different? A discussion involving statistics2.0 and computational sciences. *International Journal of Data Science and Analytics*, *6*, 167–175.

Marsland, S. (2015). *Machine learning: An algorithmic perspective*. Boca Raton, FL: CRC Press.

Mousavi, S. M., Aminian, P., Gandomi, A. H., Alavi, A. H., & Bolandi, H. (2012). A new predictive model for compressive strength of HPC using gene expression programming. *Advances in Engineering Software*, *45*(1), 105–114.

Nabian, M. A., & Meidani, H. (2018). Deep learning for accelerated seismic reliability analysis of transportation networks. *Computer-Aided Civil and Infrastructure Engineering*, *33*(6), 443–458.

Naderpour, H., Rafiean, A. H., & Fakharian, P. (2018). Compressive strength prediction of environmentally friendly concrete using artificial neural networks. *Journal of Building Engineering*, *16*, 213–219.

Nambiar, E. K. K., & Ramamurthy, K. (2008). Models for strength prediction of foam concrete. *Materials and Structures*, *41*(2), 247–254.

Nehdi, M., Djebbar, Y., & Khan, A. (2001). Neural network model for preformed-foam cellular concrete. *Materials Journal*, *98*(5), 402–409.

Neville, A. M. (2012). *Properties of concrete*. Harlow, England: Prentice Hall.

Ngo, T., Hajimohammadi, A., Sanjayan, J., & Mendis, P. (2017). Characterisation tests and design of foam concrete for prefabricated modular construction. *Concrete in Australia*, *43*(3), 43–50.

Nguyen, T., Ghazlan, A., Kashani, A., Bordas, S., & Ngo, T. (2018). 3d meso-scale modelling of foamed concrete based on x-ray computed tomography. *Construction and Building Materials*, *188*, 583–598.

Nguyen, T. T., Bui, H. H., Ngo, T. D., & Nguyen, G. D. (2017). Experimental and numerical investigation of influence of air-voids on the compressive behaviour of foamed concrete. *Materials & Design*, *130*(Supplement C), 103–119.

Nielsen, I. A. (2015). *Neural networks and deep learning*. Determination Press. http://neuralnetworksanddeeplearning.com

Pan, Z., Hiromi, F., & Wee, T. (2007). Preparation of high performance foamed concrete from cement, sand and mineral admixtures. *Journal of Wuhan University of Technology-Materials Science Edition*, *22*(2), 295–298.

Panakkat, A., & Adeli, H. (2009). Recurrent neural network for approximate earthquake time and location prediction using multiple seismicity indicators. *Computer-Aided Civil and Infrastructure Engineering*, *24*(4), 280–292.

Rafiei, M. H., & Adeli, H. (2017). A novel machine learning-based algorithm to detect damage in high-rise building structures. *Structural Design of Tall and Special Buildings*, *26*(18). https://doi.org/10.1002/tal.1400.

Rafiei, M. H., & Adeli, H. (2018). A novel unsupervised deep learning model for global and local health condition assessment of structures. *Engineering Structures*, *156*, 598–607.

Rafiei, M. H., Khushefati, W. H., Demirboga, R., & Adeli, H. (2016). Neural network, machine learning, and evolutionary approaches for concrete material characterization. *ACI Materials Journal*, *113*(6), 781–790.

Rafiei, M. H., Khushefati, W. H., Demirboga, R., & Adeli, H. (2017a). Novel approach for concrete mixture design using neural dynamics model and virtual lab concept. *ACI Materials Journal*, *114*(1), 117–128.

Rafiei, M. H., Khushefati, W. H., Demirboga, R., & Adeli, H. (2017b). Supervised deep restricted Boltzmann machine for estimation of concrete. *ACI Materials Journal*, *114*(2), 237–244.

Ramamurthy, K., Nambiar, E. K., & Ranjani, G. (2009). A classification of studies on properties of foam concrete. *Cement and Concrete Composites*, *31*(6), 388–396.

Roberts, C. A., & Attoh-Okine, N. O. (1998). A comparative analysis of two artificial neural networks using pavement performance prediction. *Computer-Aided Civil and Infrastructure Engineering*, *13*(5), 339–348.

Sadrmomtazi, A., Sobhani, J., & Mirgozar, M. (2013). Modeling compressive strength of EPS lightweight concrete using regression, neural network and ANFIS. *Construction and Building Materials*, *42*, 205–216.

Sarıdemir, M. (2009). Prediction of compressive strength of concretes containing metakaolin and silica fume by artificial neural networks. *Advances in Engineering Software*, *40*(5), 350–355.

Schmidhuber, J. (2015). Deep learning in neural networks: An overview. *Neural Networks*, *61*, 85–117.

Tam, C. T., Lim, T. Y., Sri Ravindrarajah, R., & Lee, S. L. (1987). Relationship between strength and volumetric composition of moist-cured cellular concrete. *Magazine of Concrete Research*, *39*(138), 12–18.

Wang, N., & Adeli, H. (2015). Self-constructing wavelet neural network algorithm for nonlinear control of large structures. *Engineering Applications of Artificial Intelligence*, *41*, 249–258.

Xue, Y., & Li, Y. (2018). A fast detection method via region-based fully convolutional neural networks for shield tunnel lining defects. *Computer-Aided Civil and Infrastructure Engineering*, *33*, 638–654.

Yaseen, Z. M., Deo, R. C., Hilal, A., Abd, A. M., Bueno, L. C., Salcedo-Sanz, S., & Nehdi, M. L. (2018). Predicting compressive strength of lightweight foamed concrete using extreme learning machine model. *Advances in Engineering Software*, *115*, 112–125.

Yeh, I.-C. (1998). Modeling of strength of high-performance concrete using artificial neural networks. *Cement and Concrete Research*, *28*(12), 1797–1808.

Yeh, I.-C. (2006). Analysis of strength of concrete using design of experiments and neural networks. *Journal of Materials in Civil Engineering*, *18*(4), 597–604.

Yu, B., Wang, H., Shan, W., & Yao, B. (2018). Prediction of bus travel time using random forests based on near neighbors. *Computer-Aided Civil and Infrastructure Engineering*, *33*(4), 333–350.

Zhang, Y., & Ge, H. (2013). Freeway travel time prediction using Takagi–Sugeno–Kang fuzzy neural network. *Computer-Aided Civil and Infrastructure Engineering*, *28*(8), 594–603.

Zhao, Z., & Ren, L. (2002). Failure criterion of concrete under triaxial stresses using neural networks. *Computer-Aided Civil and Infrastructure Engineering*, *17*(1), 68–73.

How to cite this article: Nguyen T, Kashani A, Ngo T, Bordas S. Deep neural network with high-order neuron for the prediction of foamed concrete strength. *Comput Aided Civ Inf*. 2019;34:316–332. https://doi.org/10.1111/mice.12422

APPENDIX A

The detailed derivation of the HO-DNN model is given as follows:

$$\delta_k^l = \frac{\partial C_{CE}}{\partial z_k^l} = \sum_j \frac{\partial C_{CE}}{\partial z_j^{l+1}} \frac{\partial z_j^{l+1}}{\partial z_k^l}$$

$$= \sum_j \delta_j^{l+1} \left[\begin{array}{l} \dfrac{\partial \sigma_1\left(z_j^{l+1,1}\right)}{\partial z_k^l} \sigma_2\left(z_j^{l+1,2}\right) \\ + \dfrac{\partial \sigma_2\left(z_j^{l+1,2}\right)}{\partial z_k^l} \sigma_1\left(z_j^{l+1,1}\right) + \dfrac{\partial \sigma_3\left(z_j^{l+1,3}\right)}{\partial z_k^l} \end{array} \right] \tag{A1a}$$

$$\frac{\partial \sigma_1\left(z_j^{l+1,1}\right)}{\partial z_k^l} = \sum_m \frac{\partial \sigma_1\left(z_j^{l+1,1}\right)}{\partial a_m^l} \frac{\partial a_m^l}{\partial z_k^l} = \frac{\partial \sigma_1\left(z_j^{l+1,1}\right)}{\partial a_k^l} \sigma'\left(z_k^l\right)$$

$$= \sum_m \frac{\partial \sigma_1\left(z_j^{l+1,1}\right)}{\partial z_m^{l+1,1}} \frac{\partial z_m^{l+1,1}}{\partial a_k^l} \sigma'\left(z_k^l\right)$$

$$= w_{jk}^{l+1,1} \sigma'_1\left(z_j^{l+1,1}\right) \sigma'\left(z_k^l\right) \tag{A1b}$$

$$\frac{\partial \sigma_2\left(z_j^{l+1,2}\right)}{\partial z_k^l} = w_{jk}^{l+1,2} \sigma'_2\left(z_j^{l+1,2}\right) \sigma'\left(z_k^l\right) \tag{A1c}$$

$$\frac{\partial a_j^{l+1,3}}{\partial z_k^l} = 2w_{jk}^{l+1,3}\sigma_3'\left(z_j^{l+1,3}\right)\sigma\left(z_k^l\right)\sigma'\left(z_k^l\right) \tag{A1d}$$

$$\frac{\partial C_{CE}}{\partial b_j^{l,1}} = \sum_k \frac{\partial C_{CE}}{\partial z_k^l}\frac{\partial z_k^l}{\partial b_j^{l,1}} = \sum_k \delta_k^l \frac{\partial \sigma\left(z_k^{l,1}\right)}{\partial b_j^{l,1}}\sigma_2\left(z_k^{l,2}\right)$$

$$= \delta_j^l \frac{\partial \sigma_1\left(z_j^{l,1}\right)}{\partial b_j^{l,1}}\sigma_2\left(z_j^{l,2}\right)$$

$$= \delta_j^l \sigma_2\left(z_j^{l,2}\right)\sum_k \frac{\partial \sigma\left(z_j^{l,1}\right)}{\partial z_k^{l,1}}\frac{\partial z_k^{l,1}}{\partial b_j^{l,1}}$$

$$= \delta_j^l \sigma'_1\left(z_j^{l,1}\right)\sigma_2\left(z_j^{l,2}\right) \tag{A2}$$

$$\frac{\partial C}{\partial w_{jk}^{l,1}} = \sum_m \frac{\partial C}{\partial z_m^l}\frac{\partial z_m^l}{\partial w_{jk}^{l,1}} = \sum_m \delta_m^l \frac{\partial \sigma_1\left(z_m^{l,1}\right)}{\partial w_{jk}^{l,1}}\sigma_2\left(z_m^{l,2}\right)$$

$$= \delta_j^l \frac{\partial \sigma_1\left(z_j^{l,1}\right)}{\partial w_{jk}^{l,1}}\sigma_2\left(z_j^{l,2}\right)$$

$$= \delta_j^l \sigma_2\left(z_j^{l,2}\right)\sum_m \frac{\partial \sigma_1\left(z_j^{l,1}\right)}{\partial z_m^{l,1}}\frac{\partial z_m^{l,1}}{\partial w_{jk}^{l,1}} \tag{A3}$$

$$= \delta_j^l \sigma'_1\left(z_j^{l,1}\right)\sigma_2\left(z_j^{l,2}\right)a_k^{l-1} \tag{A4}$$

APPENDIX B

The Data set 1, Data set 1A, Data set 2, and the developed HO-DNN model can be downloaded from https://figshare.com/s/6424e3931fd5a82bbd3a.